Manipulating the nematic director by magnetic fields in the spin-triplet superconducting state of $Cu_xBi_2Se_3$

M. Yokoyama,[*] H. Nishigaki,[*] S. Ogawa, S. Nita, H. Shiokawa, K. Matano, and Guo-qing Zheng [†]

Department of Physics, Okayama University, Okayama 700-8530, Japan

Electronic nematicity, a consequence of rotational symmetry breaking, is an emergent phenomenon in various new materials. In order to fully utilize the functions of these materials, ability of tuning them through a knob, the nematic director, is desired. Here we report a successful manipulation of the nematic director, the vector order parameter (**d** vector), in the spin-triplet superconducting state of $Cu_xBi_2Se_3$ by magnetic fields. At $H = 0.5\,\mathrm{T}$, the ac susceptibility related to the upper critical field shows a twofold symmetry in the basal plane. At $H = 1.5\,\mathrm{T}$, however, the susceptibility shows a sixfold symmetry, which has never been reported before in any superconductor. These results indicate that the **d** vector initially pinned to a certain direction is unlocked by a threshold field to respect the trigonal crystal symmetry. We further reveal that the superconducting gap in different crystals converges to p_x symmetry at high fields, although it differs at low fields.

Skyrmion spin textures of magnets [1], the normal state of iron-pnictides [2], and the superconducting states of spin-triplet superconductors [3,4] and magic-angle graphene [5] are all nematic. Furthermore, the excitation in the vortex cores of spin-triplet superconductors can form nematic skymion-type texture [6]. In particular, nematic spin-triplet superconducting states are topological [7], where Majorana fermions (excitations) are expected to appear on edges or in the vortex cores [8,9], which can potentially be applied to fault tolerant non-Abelian quantum computing [10,11]. However, bulk spin-triplet superconductors are still very rare. Carrier-doped topological insulator $Cu_{0.3}Bi_2Se_3$ [3] and ferromagnetically correlated electron system $K_2Cr_3As_3$ [4] are recently-established spin-triplet superconductors, with the superconducting transition temperature T_c as high as 6.5 K. Along with the uranium-based candidates such as UTe_2 [12], they provide good platforms for the study of topological quantum phenomena. In order to implement these compounds in applications, however, one still needs to better understand the physics of the spin-triplet states in these materials.

In contrast to spin-singlet state, a spin-triplet superconducting state is described by the vector order parameter **d**, whose direction is perpendicular to the direction of paired spins and whose magnitude is the gap size [13]. In superfluid ^{3}He, the **d** vector rotates freely [14]. In a solid, however, the **d** vector can be pinned to a certain direction which results in spin-rotation symmetry breaking as first found in $Cu_{0.3}Bi_2Se_3$ [3]. The pinning of the **d** vector is the origin of the observed nematic responses [3,15–20], so that the **d** vector is the nematic director. When the **d** vector rotates or is flipped, the magnetic response also changes and the pairing

symmetry can even change, giving rise to a transition from a phase with one symmetry to another with different symmetry. $Cu_xBi_2Se_3$ exemplifies such intriguing property, where carrier concentration tunes the superconducting phase from one to another with different **d** vector direction. For low doping level with $x < 0.46$, the **d** vector lies in the basal plane, while for high dopings with $x \geqslant 0.46$, the **d** vector rotates to the c axis direction [20,21], accompanying a possible nematic-to-chiral phase transition. Thus, a thorough understanding of the **d** vector and its interaction with the environment and external perturbations is important.

In this paper, we report a successful manipulation of the **d** vector in $Cu_xBi_2Se_3$ by a magnetic field as small as 1 tesla. We synthesized Cu-doped Bi_2Se_3 single crystals with low doping rate by the electrochemical intercalating method. Through the measurements of ^{77}Se nuclear magnetic resonance (NMR), we confirm the small carrier concentration and less disorder/defects caused by doping of the new crystals. We measure the ac susceptibility in the superconducting state by rotating the sample in a magnet to change the angle between the magnetic field and the crystal a axis. We further reveal the intrinsic gap symmetry of $Cu_xBi_2Se_3$.

Single crystals of $Cu_xBi_2Se_3$ were prepared by intercalating Cu into Bi_2Se_3 by the electrochemical doping method described in Refs. [20,22]. First, single crystals of Bi_2Se_3 were grown by melting stoichiometric mixtures of elemental Bi (99.9999%) and Se (99.999%) at $850\,^{\circ}\mathrm{C}$ for 48 hours in sealed evacuated quartz tubes. After melting, the sample was slowly cooled down to $550\,^{\circ}\mathrm{C}$ over 48 hours and kept at the same temperature for 24 hours. Those melt-grown Bi_2Se_3 single crystals were cleaved into smaller rectangular pieces of about 14 mg. They were wound by bare copper wire (diameter 0.05 mm), and used as a working electrode. A Cu wire with diameter of 0.5 mm was used both as the counter (CE) and the reference electrode (RE). We applied a current of $10\,\mu\mathrm{A}$ in a saturated solution of CuI powder (99.99%) in acetonitrile

---

[*]Partly based on Master's degree thesis by M. Yokoyama (Feb. 2021) and H. Nishizaki (Feb. 2022), Okayama University.
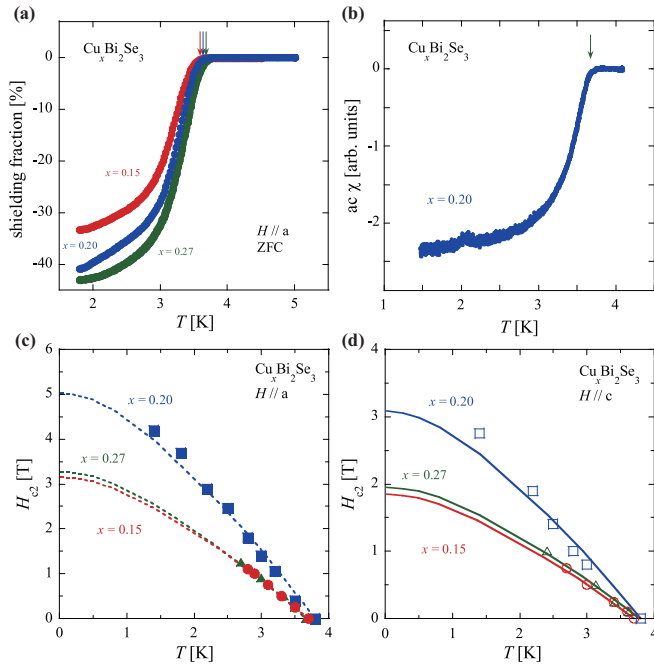
[†]zheng@psun.phys.okayama-u.ac.jp

FIG. 1. (a) Superconducting transition and the shielding fraction of $Cu_xBi_2Se_3$ ($x = 0.15$, 0.20, and 0.27). Arrows indicate T_c for the samples. (b) ac susceptibility for the sample with $x = 0.20$. A small hump around $T = 2.1$ K is due to the environmental change associated with the superfluid transition of liquid helium. (c) upper critical field H_{c2} for $H \parallel a$ for the three samples, (d) H_{c2} for $H \parallel c$ for the three samples.

(CH$_3$CN). The obtained crystals samples were then annealed at $560\,^{\circ}$C for 1 hour in sealed evacuated quartz tubes, and quenched into water. After quenching, the samples were covered with epoxy (STYCAST 1266) to avoid deterioration. We have confirmed that the epoxy does not have extrinsic effect on the physical properties such as T_c or upper critical field H_{c2}. The Cu concentration x was determined from the mass increment of the samples. To check the superconducting properties, dc susceptibility measurements were performed using a superconducting quantum interference device (SQUID) with the vibrating sample magnetometer (VSM). The ^{77}Se -NMR spectra were obtained by the fast Fourier transformation of the spin-echo at a field of $H_0 = 1.5$ T. The Knight shift K was calculated using nuclear gyromagnetic ratio $\gamma_N = 8.118$ MHz/T for ^{77}Se. The ac susceptibility was measured by the inductance of an *in situ* NMR coil. Angle-dependent measurements were performed by using a piezo-driven rotator (Attocube ANR51) equipped with Hall sensors to determine the angle between magnetic field and crystal axis. We estimate that the error in the angle determination is less than 1 degree. Figure 1(a) shows the superconducting transition of the three samples $Cu_xBi_2Se_3$ ($x = 0.15$, 0.20, and 0.27) obtained by dc susceptibility measurements. The T_c is 3.6, 3.8, and 3.6 K for $x = 0.15$, 0.20, and 0.27, respectively, which is higher than T_c of other x concentrations reported for $x \geqslant 0.28$, following a general trend that T_c increases with decreasing x [20,23]. The shielding fraction at $T = 1.8$ K for $x = 0.20$ and 0.27 exceeds 40% which is among the highest value reported so far. In our case, demagnetization is negligible as the magnetic
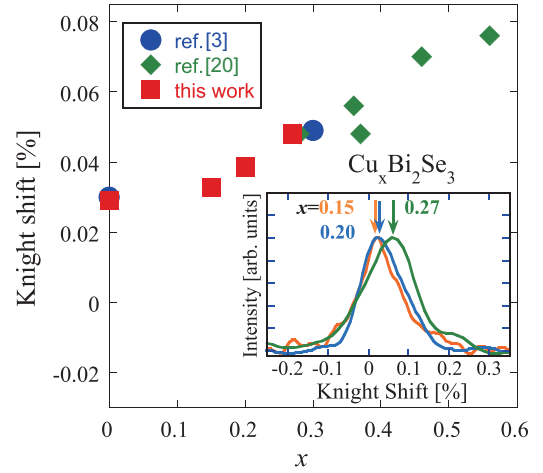

FIG. 2. The ^{77}Se Knight shift as a function of nominal Cu-content x. The inset shows the NMR spectrum for $x = 0.15$, 0.20, and $x = 0.28$. The arrow indicates the gravity center of the spectrum from which the Knight shift was extracted.

field is applied parallel to the plate. Figure 1(b) shows the data for $x = 0.20$ as a representative example for ac susceptibility. Figures 1(c) and 1(d) show the upper critical field H_{c2} for $H \parallel a$ and $H \parallel c$, respectively. The H_{c2} for $x = 0.15$ and 0.27 is comparable to that reported previously by Kriener *et al.* [23], but H_{c2} for $x = 0.20$ is much higher. In Fig. 2, we show the ^{77}Se Knight shift as a function of Cu-content x for these samples, together with the data for other samples reported previously [3,20]. The Knight shift, which is proportional to the density of states, decreases with decreasing x, being consistent with a smaller carrier concentration for the new crystals than that for the previous ones with $x \geqslant 0.28$. The ^{77}Se -NMR spectrum taken at $H = 1.5$ T and $T = 3.0$ K above $T_c(H)$ was shown in the inset to the figure. The spectrum becomes sharper with decreasing x, with the full width at half maximum (FWHM) of 14.4 kHz and 14.7 kHz for $x = 0.15$ and $x = 0.20$, respectively, which is narrower than that for $x = 0.27$ (16.5 kHz) and $x \geqslant 0.28$ [3,20] and thus ensures that these low-doping samples have less disorder.

Figures 3–5 show the main results of this work. Figures 3(a), 4(a), and 5(a) depict the angle φ dependence of the diamagnetism measured by ac susceptibility at $T = 1.4$ K [see Fig. 1(b) for an example] under various magnetic fields. Here φ is the angle between the crystal a axis and the magnetic field. The predetermined a axis direction is set to be $\varphi = 0$ degrees. The plotted quantity is related to H_{c2}; the larger H_{c2}, the larger diamagnetism at a fixed temperature and field. At $H = 0.5$ T, a (nearly) twofold symmetry is observed, in agreement with previous Knight shift [3] and H_{c2} [3,15,20] measurements. At $H = 1.15$ T (1.25 T for $x = 0.20$ and 1 T for $x = 0.27$), new components emerge in the oscillation, and surprisingly, there emerges six minima in the oscillation at $H = 1.5$ T. The situation is better visualized in the polar plots in Figs. 3(b), 4(b), and 5(b). A sixfold symmetry is clearly seen at $H = 1.5$ T.

The data in the lower panel of Fig. 3(b) can be fitted by a phenomenological formula $-\chi = -\dfrac{|\chi_{\max}|}{\sqrt{\cos^2(\varphi-\theta)+c\cdot\sin^2(\varphi-\theta)}}$. Here, $|\chi_{\max}|$ is the largest diamagnetic susceptibility and θ is
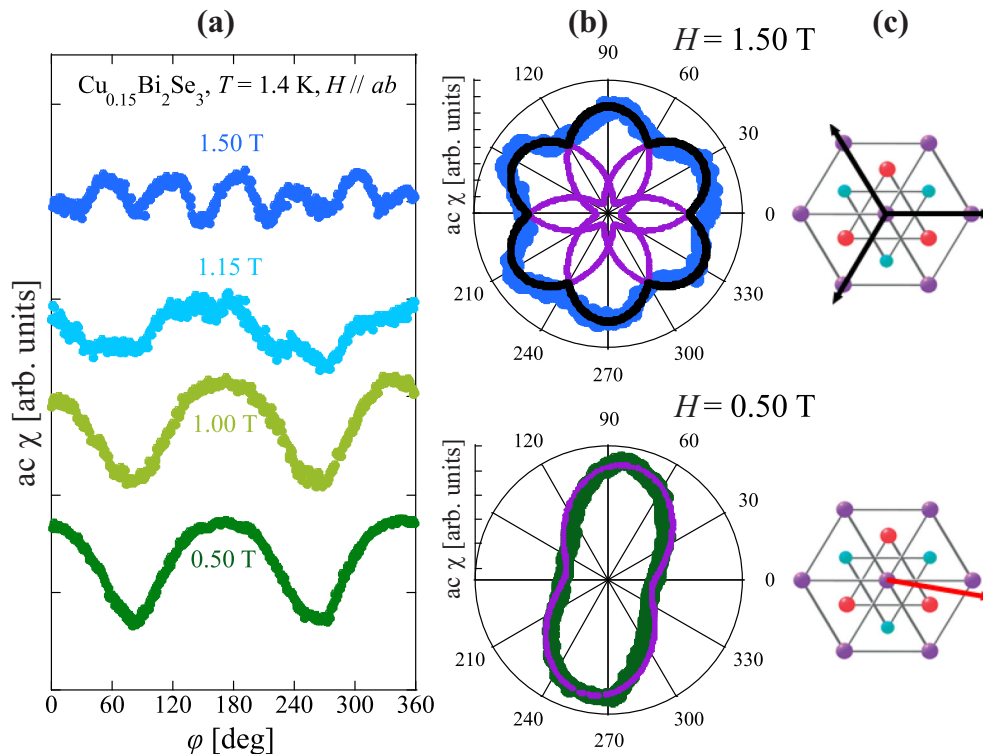
FIG. 3. Field- and angle-evolution of the diamagnetism and **d** vector revealed by the ac susceptibility measurement for $x = 0.15$. (a) In-plane angle dependence of the diamagnetism at $T = 1.4$ K measured by the ac susceptibility under various fields. (b) Polar plot of the ac susceptibility at $H = 0.5$ T and 1.5 T, respectively. The purple curve in the lower panel is a simulation of an anisotropic H_{c2} formula (see text). In the upper panel, the black curve connects the outer envelope of the three ellipses. (c) Illustration of the **d** vector(s) by arrow(s) at different fields. The purple balls depict Bi, and the red and green balls represent Se in the bird's-eye view basal planes.

the angle between the elliptical direction and the a axis, and c is a number parameter that determines the shape of the ellipse. The parameter c obtained from the fittings in Figs. 3(b), 4(b), and 5(b) is 1.3, 1.2, and 1.4, respectively. A smaller c makes the shape more peanutlike while a larger c makes the shape more ellipselike. This formula was originally developed to describe the H_{c2} anisotropy [25] and was also adapted in Ref. [16].

Although the data for $x = 0.15$ agree well with the simulation of a single ellipse (a single component), the data for $x = 0.20$ and 0.27 do not. There is a small second component, as can be seen in the lower panels of Figs. 4(b) and 5(b). For $x = 0.20$, the θ for the small, second component is 340°, while it is 80° for the main component. For $x = 0.27$, the θ is 355° for the main component, and 95° for the second component. In either case, the subdominant component disappears at high fields beyond 1.5 T, which indicates that it arises from a different crystal domain with a lower H_{c2} (see below for more discussion). The single domain seen in $x = 0.15$ can be understood as due to its lower doping which makes the crystal more homogeneous as evidenced by the sharper NMR spectrum. Theoretically, two degenerate gap states corresponding to p_x and p_y were proposed by Fu [26]. The main component for $x = 0.15$ and $x = 0.20$ is compatible with p_x, but that for $x = 0.27$ is compatible with p_y symmetry. In the previous work, H_{c2} measurements found that $x = 0.3$ and 0.37 correspond to p_x while $x = 0.28$ and 0.36 correspond to p_y [3,20].

Looking into the detail of the lower panels of Figs. 3(b), 4(b), and 5(b), one notices that the elliptical axis is tilted away from the high-symmetry (crystal axis) direction. As the **d** vector is perpendicular to the main axis of the H_{c2} ellipse [3,20], we illustrate the corresponding **d** vector for the present three crystals in the lower panels of Figs. 3(c), 4(c), and 5(c). For $x = 0.20$, the **d** vector for the main component is tilted from the high symmetry axis by $\delta = -10°$, while the tilting angle is $\delta = 10°$ for the sub-dominant component. So the two components can be regarded as belonging to the same gap symmetry in view of the trigonal crystal symmetry. For $x = 0.27$, the **d** vector is 85°, which is close to 90°, for the main component, while it is 5° for the minor component. Therefore, the two components correspond to different symmetries that are orthogonal to each other. We believe that the cause for the tilting from the high-symmetry axis direction is phonon-mediated interaction. Hecker and Fernandes [27] recently proposed that the competition between a quadratic phonon-mediated interaction $E_{\text{nem−ph}}$ and the cubic nematic anharmonicity can make the nematic director deviate from the high-symmetry direction. The intrinsic nematic anharmonic cubic interaction E_{nem} favors the nematic director to align parallel to the high-symmetry directions, while the phonon-mediated nonanalytic quadratic interaction prefers the nematic director to align to the directions farthest away from the high-symmetry directions.

Hecker and Fernandes further pointed out that the phonon interaction and thus the nematic director (**d** vector) rotation
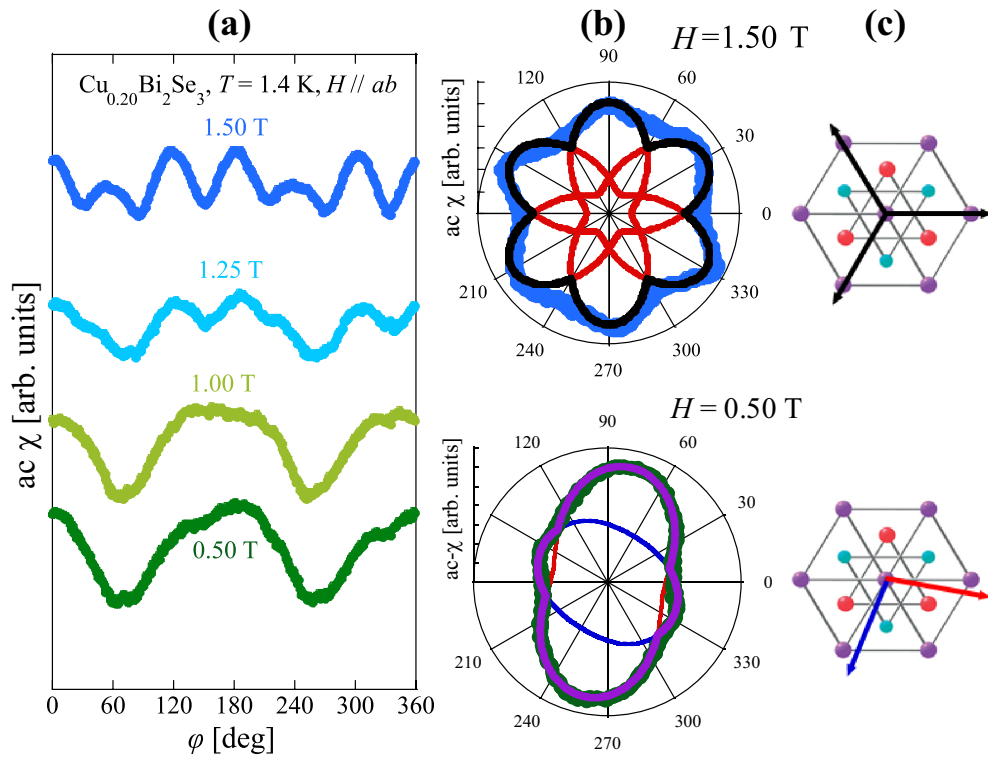
FIG. 4. (a) In-plane angle dependence of the ac susceptibility of the $x = 0.20$ crystal at $T = 1.4$ K for various fields. (b) Polar plot of the ac susceptibility at $H = 0.5$ T and 1.5 T. In the lower panel, red and blue curves are the simulations of the ac χ from two different domains. The thick purple curve is the outer envelop of the two ellipses. For other versions of the simulation curves, see Supplemental Material [24] (c) Illustration of the **d** vector direction(s).
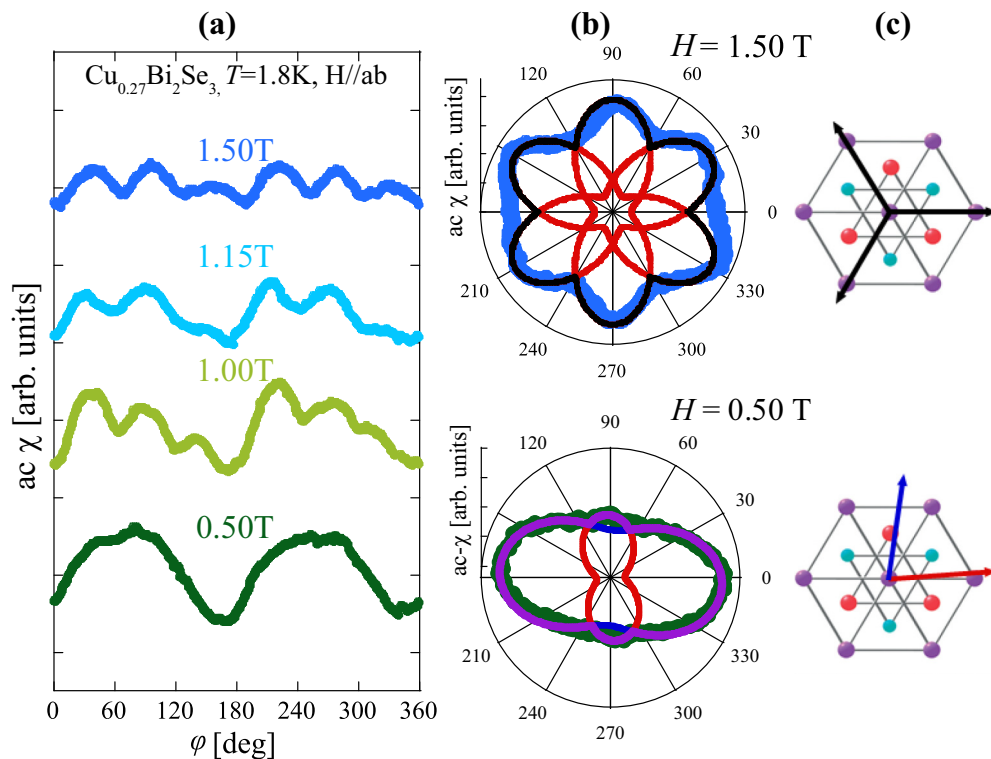

FIG. 5. Field- and angle-evolution of the diamagnetism and **d** vector for $x = 0.27$. (a) In-plane angle dependence of the diamagnetism at $T = 1.8$ K measured by the ac susceptibility under various fields for $x = 0.27$. (b) Polar plot of the ac susceptibility at $H = 0.5$ T and 1.5 T, respectively. The captions for the curves are the same as Fig. 4(b). (c) Illustration of the **d** vector direction(s) at different fields.

will have an impact on domain formations [27]. If the **d** vector is along the high symmetry axis, the three equivalent directions have the same angular separation, and the surface energies between any two domains are equal. As a result, when one direction among the three is chosen as the majority-domain **d** vector, the other two directions will be randomly picked as minority-domain **d** vectors [27]. However, if the **d** vector is rotated by an angle δ away from the crystal axis, in order to minimize the surface energy, then there will only be one type of minor domain with the **d** vector rotated by an angle of $-\delta$. This is exactly we have found for the $x = 0.20$ crystal.

At low fields, the twofold nematic behavior in the physical quantities is well understood as due to the **d** vector pinning to a certain direction by, *e.g.*, spin-orbit coupling promoted by disorder or defects, although there are three equivalent directions favored by the **d** vector. In superfluid ^{3}He, the **d** vector rotates freely as there is no lattice. As can be seen in Figs. 3–5, the oscillation in H_{c2} restores a sixfold symmetry at high fields of $H \geqslant 1.5$ T, compatible with the trigonal crystal-lattice symmetry. Namely, the three a-axis directions become equivalent at high fields, as depicted in the upper panels of Figs. 3(c), 4(c), and 5(c). This means that the **d** vector is depinned by the application of a large magnetic field. We should note that a possible change in vortex lattice structure cannot explain the observed symmetry change. Firstly, any vortex lattice cannot give rise to a twofold symmetry in physical quantities. Secondly, a higher order effect could lead to a response of sixfold symmetry at high fields in principle, but in such case a circularlike shape should appear at low fields [28], which is not seen in our experiments.

The simplest interpretation of the symmetry transition in H_{c2} is through the total energy $E_{tot} = E_{nem} + E_{nem-ph} + E_{Zeeman}$ including Zeeman energy E_{Zeeman}. Above a threshold value H_{pin}, the **d** vector traces the rotating magnetic field as to gain Zeeman energy which is the largest when the **d** vector is perpendicular to the field. The energy gain by E_{nem} is the largest when the **d** vector is along the three high-symmetry directions. The H_{pin} is $1.0 \sim 1.2$ T in the case of $Cu_xBi_2Se_3$. This is the first case, to our knowledge, that the **d** vector can be manipulated by the magnetic field. Also, a sixfold symmetry of H_{c2} or its related physical quantities has never been observed before in any superconductor, although theories have pointed out that a trigonal superconductor with a two-component order parameter may show such property under certain conditions [29,30]. Therefore, our result is supplemental to the Knight shift measurement which revealed a spin-triplet state in $Cu_xBi_2Se_3$.

The most intriguing feature is that, although the long axis direction of the ellipse for the angle-dependent Meissner diamagnetism is tilted way from the high symmetry axis

directions of the trigonal crystal lattice at low fields, with $\theta = 80°$ for $x = 0.15$ and $x = 0.20$, it is restored to the high symmetry axis directions at high fields $H \geqslant 1.5$ T. This means that the phonon-induced interaction E_{nem-ph} is also smaller than the Zeeman interaction. Such symmetry at high magnetic fields is compatible with the so-called Δ_{4x} (p_x) state proposed [26]. In contrast, the ellipse for $x = 0.27$ at low fields has an elliptical direction along $\theta = 355°$ and thus the gap is compatible with the other state, the so-called Δ_{4y} (p_y) state. The previously reported crystals of $x = 0.28$ and 0.36 also showed such symmetry. Most strikingly and surprisingly, the Δ_{4y} (p_y) compatible elliptical shape at low fields is also restored to the symmetry of Δ_{4x} (p_x) at high fields, as seen in the upper panels of Figs. 5(b) and 5(c). We have investigated more than 16 crystals with $0.15 \leqslant x \leqslant 0.40$, and found that all of them become compatible with the Δ_{4x} state after the **d** vector is depinned at high magnetic fields, although the θ is different from crystal to crystal at low fields and some of them are consistent with the Δ_{4y} symmetry. This implies that the intrinsic gap symmetry is Δ_{4x}. We speculate that the Δ_{4y} appearing in some cases is accidental due to local defects caused by the quenching process. This is an open question that needs to be addressed in the future.

In conclusion, for the first time, we have successfully manipulated the nematic director by magnetic fields. The diamagnetism in single crystal samples of $Cu_xBi_2Se_3$ measured by ac susceptibility shows a twofold symmetry with respect to the angle between the field and the crystal a axis at a low field $H = 0.5$ T, with the direction of largest diamagnetism slightly deviated from the crystal axis. At high fields of $H \geqslant 1.5$ T, however, the ac susceptibility shows a sixfold symmetry, exactly matching the crystal axes. These results indicate that the **d** vector initially pinned to a certain direction is unlocked by the magnetic fields above a threshold value to trace the field. The sixfold symmetry in H_{c2} or its related physical quantities was expected for a spin-triplet superconductor with two-component order parameter, but has never been observed before. Thus, our results are supplemental to the Knight shift result which found that $Cu_xBi_2Se_3$ is a spin-triplet superconductor. Our work further reveals the p_x gap symmetry at high fields for all samples, irrespective of different symmetries at low fields, indicating that this is the intrinsic gap symmetry of $Cu_xBi_2Se_3$.

[1] U. K. Rößler, A. N. Bogdanov, and C. Pfleiderer, Spontaneous skyrmion ground states in magnetic metals, Nature **442**, 797 (2006).

[2] R. M. Fernandes, A. V. Chubukov, and J. Schmalian, What drives nematic order in iron-based superconductors? Nat. Phys. **10**, 97 (2014).

[3] K. Matano, M. Kriener, K. Segawa, Y. Ando, and G.-q. Zheng, Spin-rotation symmetry breaking in the superconducting state of $Cu_xBi_2Se_3$, Nat. Phys. **12**, 852 (2016).

[4] J. Yang, J. Luo, C. J. Yi, Y. G. Shi, Y. Zhou, and G.-q. Zheng, Spin-triplet superconductivity in $K_2Cr_3As_3$, Sci. Adv. **7**, eabl4432 (2021).

[5] Y. Cao, D. Rodan-Legrain, J. M. Park, N. F. Q. Yuan, K. Watanabe, T. Taniguchi, R. M. Fernandes, L. Fu, and P. Jarillo-Herrero, Nematicity and competing orders in superconducting magic-angle graphene, Science **372**, 264 (2021).

[6] A. A. Zyuzin, J. Garaud, and E. Babaev, Nematic Skyrmions in Odd-Parity Superconductors, Phys. Rev. Lett. **119**, 167001 (2017).

[7] L. Fu and E. Berg, Odd-Parity Topological Superconductors: Theory and Application to $Cu_xBi_2Se_3$, Phys. Rev. Lett. **105**, 097001 (2010).

[8] X.-L. Qi and S.-C. Zhang, Topological insulators and superconductors, Rev. Mod. Phys. **83**, 1057 (2011).

[9] D. A. Ivanov, Non-Abelian Statistics of Half-Quantum Vortices in *p*-Wave Superconductors, Phys. Rev. Lett. **86**, 268 (2001).

[10] M. H. Freedman, A. Kitaev, M. J. Larsen, and Z. Wang, Topological quantum computation, Bull. Am. Math. Soc. **40**, 31 (2003).

[11] A. Kitaev, Fault-tolerant quantum computation by anyons, Ann. Phys. **303**, 2 (2003).

[12] S. Ran, C. Eckberg, Q.-P. Ding, Y. Furukawa, T. Metz, S. R. Saha, I.-L. Liu, M. Zic, H. Kim, J. Paglione, and N. P. Butch, Nearly ferromagnetic spin-triplet superconductivity, Science **365**, 684 (2019).

[13] R. Balian and N. R. Werthamer, Superconductivity with Pairs in a relative p wave, Phys. Rev. **131**, 1553 (1963).

[14] A. J. Leggett, A theoretical description of the new phases of liquid ^{3}He, Rev. Mod. Phys. **47**, 331 (1975).

[15] S. Yonezawa, K. Tajiri, S. Nakata, Y. Nagai, Z. Wang, K. Segawa, Y. Ando, and Y. Maeno, Thermodynamic evidence for nematic superconductivity in $Cu_xBi_2Se_3$, Nat. Phys. **13**, 123 (2017).

[16] Y. Pan, A. M. Nikitin, G. K. Araizi, Y. K. Huang, Y. Matsushita, T. Naka, and A. de Visser, Rotational symmetry breaking in the topological superconductor $Sr_xBi_2Se_3$ probed by upper-critical field experiments, Sci. Rep. **6**, 28632 (2016).

[17] T. Asaba, B. J. Lawson, C. Tinsman, L. Chen, P. Corbae, G. Li, Y. Qiu, Y. S. Hor, L. Fu, and L. Li, Rotational Symmetry Breaking in a Trigonal Superconductor Nb-doped Bi_2Se_3, Phys. Rev. X **7**, 011009 (2017).

[18] G. Du, Y. Li, J. Schneeloch, R. D. Zhong, G. Gu, H. Yang, H. Lin, and H.-H. Wen, Superconductivity with two-fold symmetry in topological superconductor $Sr_xBi_2Se_3$, Sci. China Phys. Mech. Astron. **60**, 037411 (2017).

[19] R. Tao, Y.-J. Yan, X. Liu, Z.-W. Wang, Y. Ando, Q.-H. Wang, T. Zhang, and D.-L. Feng, Direct Visualization of the Nematic Superconductivity in $Cu_xBi_2Se_3$, Phys. Rev. X **8**, 041024 (2018).

[20] T. Kawai, C. G. Wang, Y. Kandori, Y. Honoki, K. Matano, T. Kambe, and G.-q. Zheng, Direction and symmetry transition of the vector order parameter in topological superconductors $Cu_xBi_2Se_3$, Nat. Commun. **11**, 235 (2020).

[21] J. W. F. Venderbos, V. Kozii, and L. Fu, Odd-parity superconductors with two-component order parameters: Nematic and chiral, full gap, and Majorana node, Phys. Rev. B **94**, 180504(R) (2016).

[22] M. Kriener, K. Segawa, Z. Ren, S. Sasaki, S. Wada, S. Kuwabata, and Y. Ando, Electrochemical synthesis and superconducting phase diagram of $Cu_xBi_2Se_3$, Phys. Rev. B **84**, 054513 (2011).

[23] M. Kriener, K. Segawa, S. Sasaki, and Y. Ando, Anomalous suppression of the superfluid density in the $Cu_xBi_2Se_3$ superconductor upon progressive Cu intercalation, Phys. Rev. B **86**, 180505(R) (2012).

[24] See Supplemental Material http://link.aps.org/supplemental/10.1103/PhysRevB.107.L100505 for the curves of the individual ellipse and the outer envelope alone.

[25] R. C. Morris, R. V. Coleman, and R. Bhandarit, Superconductivity and Magnetoresistance in $NbSe_2$, Phys. Rev. B **5**, 895 (1972).

[26] L. Fu, Odd-parity topological superconductor with nematic order: Application to $Cu_xBi_2Se_3$, Phys. Rev. B **90**, 100509(R) (2014).

[27] M. Hecker and R. M. Fernandes, Phonon-induced rotation of the electronic nematic director in superconducting Bi_2Se_3, Phys. Rev. B **105**, 174504 (2022).

[28] M. Ichioka, N. Enomoto, and K. Machida, Vortex lattice structure in a $d_{x^2-y^2}$-wave superconductor, J. Phys. Soc. Jpn. **66**, 3928 (1997).

[29] J. W. F. Venderbos, V. Kozii, and L. Fu, Identication of nematic superconductivity from the upper critical field, Phys. Rev. B **94**, 094522 (2016).

[30] P. L. Krotkov and V. P. Mineev, Upper critical field in a trigonal unconventional superconductor: UPt_3, Phys. Rev. B **65**, 224506 (2002).